

# Creation and detection of the topological insulating phase in Bi<sub>4</sub>I<sub>4</sub>

Hideaki Murase<sup>1</sup>, Kazuhiro Takeda<sup>2</sup>

<sup>1</sup> *Dept. of Appl. Phys. Kanoda Lab.*

<sup>2</sup> *Dept. of Appl. Phys. Kagawa Lab.*

## Author

Hideaki Murase: His research field is solid state physics of charge glass in organic conductors. Here, he is responsible for measuring and analysis.

Kazuhiro Takeda: His research field is controlling of non-equilibrium quantum states by Raman spectroscopy. Here, he is responsible for setup, measuring and analysis.

## Abstract

Supercooling, one of non-equilibrium phenomena, is expected to bring about hidden quantum phases and to be available for the development of new devices through the phase control. Here, we initially tried to generate the supercooled quantum phase of Bi<sub>4</sub>I<sub>4</sub> at low temperatures; however, it was unsuccessful because of the problem of the sample degradation. Then, we changed the target material to the organic conductor,  $\theta$ -(ET)<sub>2</sub>TiCo(SCN)<sub>4</sub> to explore the microscopic nature of the charge glass, which is realized by supercooling the charge liquid state.

When cooling Bi<sub>4</sub>I<sub>4</sub> slowly around room temperature, it undergoes a phase transition from a topological insulator (TI) to a normal insulator (NI) at 298 K. The TI can be stabilized as a nonequilibrium metastable phase at low temperatures well below 298 K if the phase transition is prevented by rapid cooling. Because the boundaries between coexisting TI and NI domains carry high conductivity, controlling TI/NI domains in real space is crucial for the development of new devices exploiting the domain-boundary engineering. The final goal of this research was to control TI/NI domains in real space, visualize them, and probe the domain boundaries through electric resistance measurements. First, we tried to detect the topological phase under slow cooling and rapid cooling conditions through Raman spectroscopy.

We constructed an experimental setup which enables us to cool the samples at a rate of about 10<sup>2</sup> K/s. The Raman spectra were observed under the condition that the sample is expected to be in the  $\beta$  phase; however, the spectra did not reproduce the previously observed profile. This is very probably due to the deterioration of the sample; then, we could not advance the present research because the observation of the reliable Raman spectrum of Bi<sub>4</sub>I<sub>4</sub> crystal was the start point of this research plan.

Since we could not have the prospect of obtaining a new sample, we stopped continuing the project using the Bi<sub>4</sub>I<sub>4</sub> sample. Then, we sought for other possible research plans exploiting the quenching technology developed so far in this research and decided to take up the organic conductor,  $\theta$ -

(ET)<sub>2</sub>TiCo(SCN)<sub>4</sub> described below, aiming to clarify the electronic state of the supercooled phase by measuring the Raman spectra as the new goal for this research.

The organic conductors,  $\theta$ -(ET)<sub>2</sub>MM'(SCN)<sub>4</sub> (MM'=TiCo and RbZn) (denoted  $\theta$ -TiCo and  $\theta$ -RbZn hereafter), consist of insulating MM'(SCN)<sub>4</sub> layers and conducting ET layers, where ET molecules form charge-frustrated anisotropic triangular lattices. Both materials are in charge liquid (CL) states at high temperatures and undergo transitions to charge order (CO) states at low temperatures. Remarkably, however, when these systems are rapidly cooled, the CG's are supercooled even below the transition temperature and charge glass (CG) states result. In the CL and CG phases, anomalously slow charge fluctuations peculiar to glass are observed [4,5]; however, the CL and CG phases exhibit several orders of magnitude higher electrical conductivity than expected from the time scale of the charge fluctuations. In other words, the CL and CG states appear to possess dual characters of electrons, high itineracy as in typical organic conductors and glassy-like localization. How these contradictory characters coping with each other in a single material are significant issues.

Previously, we performed Raman spectroscopy measurements of  $\theta$ -RbZn in the CL phase and analyzed the spectral shape to know the charge density distribution in the system. As a result, it was clarified that the CL phase of  $\theta$ -RbZn has a charge density profile having a peak at  $\rho=0.5$  and continuously decreasing towards both sides of  $\rho=0$  and 1. This result suggests that the charge location in the CG phase of  $\theta$ -RbZn is not particle-like but wave-like; so to speak, like a quantum glass.

The CG phase in  $\theta$ -TiCo, which has weaker charge frustration than  $\theta$ -RbZn, is of great interest to see the relation between the charge density profile and the degree of charge frustration. The CG phase of  $\theta$ -TiCo has, however, hardly been studied so far since  $\theta$ -TiCo has a low glass-forming ability than  $\theta$ -RbZn and requires very high cooling speeds for quenching the high-temperature CL state. Here, we tried to realize the CG phase by applying the quenching technique developed in the Bi<sub>4</sub>I<sub>4</sub> experiment to  $\theta$ -TiCo. As a result, we succeeded in stabilizing the CG phase of  $\theta$ -TiCo, measuring the Raman spectrum of it, and deducing the charge density distribution from the analysis of the spectrum. The charge density of the CG phase of  $\theta$ -TiCo has two peaks at  $\rho=0.1$  and 0.9 with a broad component around  $\rho=0.5$  in contrast to the single-peak profile in  $\theta$ -RbZn. This particle-like character of the charge location means that the CG of  $\theta$ -TiCo is more classical than that of  $\theta$ -RbZn. This suggests that the nature of the charge glass changes from classical to quantum as frustration increases.

## 1. Creation and detection of the topological insulating phase in Bi<sub>4</sub>I<sub>4</sub>

### Background and purpose

Conventional studies on quantum solid state physics have mainly focused on equilibrium states of matters; however, few studies have been conducted on non-equilibrium states. Here, we investigate one of the non-equilibrium phenomena, supercooling, where a high-temperature phase is stabilized as

a metastable state even below the transition temperature. Supercooling enables hidden quantum phases and properties to emerge. Therefore, supercooling provides a unique state-controlling method in non-equilibrium quantum solid state physics and development of new devices based on new principles.

When cooling  $\text{Bi}_4\text{I}_4$  around room temperature, it undergoes a structural phase transition from the  $\beta$  phase of TI to the  $\alpha$  phase of NI [1,2]. The phase transition can be prevented by quenching the system, and the  $\beta$  phase can be stabilized as a supercooled phase even below the transition temperature. TI and NI are both insulators; however, their domain boundaries carry high electrical conductivity, so controlling the domains in real space is crucial for applying TI to devices. The final goal of this study is to control the TI/NI domains in real space, visualize them, and probe the domain boundaries through electrical resistance measurements. First, we tried to detect the topological phase of  $\text{Bi}_4\text{I}_4$  under rapid cooling and slow cooling conditions through Raman spectroscopy.

## Experimental

Since the transition of the topological phase of  $\text{Bi}_4\text{I}_4$  is accompanied by the transition of the crystal structure, we tried to detect it by Raman spectroscopy. A WITEC system was used for Raman spectroscopy, and an attocube system was used for real-space scanning. The optical system consists of a  $\lambda/2$  wavelength plate (Thorlabs, LP03-532RE-25) for controlling the polarization of the excitation light and a bandpass filter (Chroma, RET532 / 4x) for sharpening the wavelength of the excitation light, long-pass filter for excluding Rayleigh scattering (IRIDIAN, 532USLPF and Semrock, LP03-532RE-25), objective lens for collecting laser light, and a grating with 1800 l/mm. A 532 nm laser polarized parallel to the b-axis of  $\text{Bi}_4\text{I}_4$  was used as the excitation light. Raman spectra was collected with backscattering geometry. The accumulation time is 60 seconds.

Since the formation of the supercooled  $\beta$  phase requires a high cooling rate, we constructed an experimental setup that allows temperature control over a small area (Fig. 1). By arranging the sapphire substrate on the resin substrate having low thermal conductivity, the sapphire substrate was insulated thermally from the environment. A thermometer, a heater, and a silicon substrate were placed on the sapphire substrate, and  $\text{Bi}_4\text{I}_4$  crystals were further placed on the silicon substrate. With this setup, we achieved a cooling rate of  $10^2$  K/s. The typical size of the  $\text{Bi}_4\text{I}_4$  crystal is ca.  $0.1 \text{ mm} \times 0.1 \text{ mm} \times 1 \text{ mm}$ .

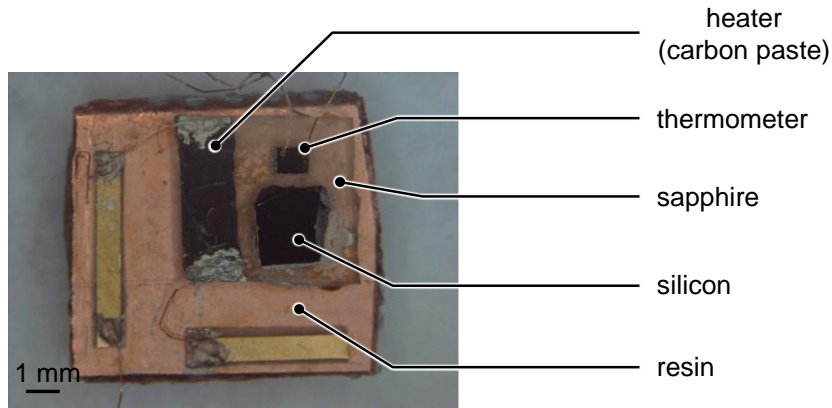


Figure 1 Photograph of the setup. A sapphire substrate is placed on the resin substrate, and a heater, a thermometer, and a sample are arranged on the sapphire substrate. The lower left scale bar indicates 1 mm.

## Result and discussion

Raman spectra near the transition temperature of  $\text{Bi}_4\text{I}_4$  were measured. Figure 2 (a) shows the Raman spectra at various temperatures when slowly cooling from 315 K. Figure 2 (b) shows the Raman spectra at 30 K under slow cooling ( $\sim 10^{-2}$  K/s) and rapid cooling ( $\sim 10^2$  K/s). Quenching was performed by heating the sample to 315 K with a heater mounted on a sapphire substrate and then turning off the heater.

The sample is expected to be in the  $\beta$  phase above the transition temperature (298 K) or below the transition temperature under quenching. Although at temperatures above the transition temperature a part of the peaks is reduced by the long pass filter, peaks exist at  $83\text{ cm}^{-1}$  and  $148\text{ cm}^{-1}$  (Fig. 2 (a)). The Raman spectrum at 30 K under quenching has peaks at  $88\text{ cm}^{-1}$  and  $153\text{ cm}^{-1}$ . According to previous studies [3], the Raman spectrum of the  $\beta$  phase between  $80\text{ cm}^{-1}$  and  $200\text{ cm}^{-1}$  with peaks only at  $96\text{ cm}^{-1}$  ( $A_g$ ) and  $115\text{ cm}^{-1}$  ( $B_g$ ) was observed. The Raman spectrum obtained in this study under the condition that the sample is expected to be in the  $\beta$  phase is inconsistent with the previous studies even when the temperature dependence of the peak position is taken into consideration.

The sample is expected to be in  $\alpha$  phase below the transition temperature under slow cooling. The Raman spectrum below the transition temperature in Fig. 2 (a) shows almost the same shape as that above the transition temperature. In addition, the Raman spectrum at 30 K under slow cooling shows almost the same shape as that under quenching.

Since the Raman spectrum of the  $\beta$  phase does not reproduce the previous study, the  $\text{Bi}_4\text{I}_4$  crystal used in this study does not have the intrinsic crystal structure from the surface to at least the penetration length of the excitation light. This is very probably due to the deterioration of the sample. Although Raman spectrum of the  $\alpha$  phase was not measured in the previous study and cannot be directly compared with this study, it is probably due to the same reason that the change in Raman spectrum

could not be confirmed near the transition temperature and at 30 K under slow cooling and rapid cooling.

Considering that the sample may deteriorate only on the surface, we tried to cleave by the Scotch tape method. However, the cleaved sample could not be placed on the substrate and the Raman spectrum could not be observed.

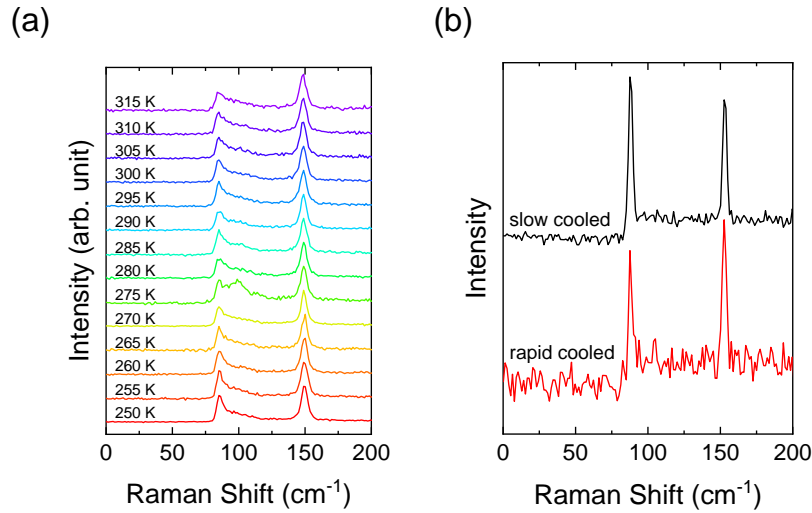


Figure 2 Raman spectra of  $\text{Bi}_4\text{I}_4$ . (a) Raman spectra of various temperatures near the transition temperature.  $\text{Bi}_4\text{I}_4$  is a topological insulator ( $\beta$  phase) at high temperature and a normal insulator ( $\alpha$  phase) at low temperature, and its transition temperature is 298 K. (b) Raman spectra at 30 K under slow cooling (black line) and rapid cooling (red line).

## Conclusion and prospect

The Raman spectra of  $\text{Bi}_4\text{I}_4$  observed in this research under the conditions that the sample is expected to be in the  $\beta$  phase did not reproduce the previous study. This result indicates that the  $\text{Bi}_4\text{I}_4$  crystal used in this study did not have the intrinsic crystal structure from the surface to at least the penetration length of the excitation light. This is very probably due to the deterioration of the sample.

In the future, we will resynthesize the sample, confirm that the Raman spectrum reproduces the previous research, and then detect the topological phase under rapid cooling and slow cooling conditions. After that, we will try to create and control NI and TI domains using a laser, visualize them in real space through a Raman imaging method, and probe the domain boundaries through electrical resistance measurements.

## 2. Analysis of charge density distribution in the charge liquid phase in $\theta\text{-(ET)}_2\text{TlCo(SCN)}_4$ by Raman spectroscopy

Since we could not have the prospect of obtaining a new sample, we stopped continuing the project

using the Bi<sub>4</sub>I<sub>4</sub> sample. Then, we sought for other possible research plans exploiting the quenching technology developed so far in this research and decided to take up the organic conductor,  $\theta$ -TlCo described below, aiming to clarify the electronic state of this supercooled phase through the Raman spectroscopy measurements as a new goal for this research.

## Background and purpose

The organic conductors,  $\theta$ -TlCo and  $\theta$ -RbZn, consist of insulating inion layers and conducting ET layers, where ET molecules form a charge-frustrated isotropic triangular lattices. Both materials are in charge liquid (CL) states at high temperatures and undergo transitions to charge order (CO) states at low temperatures. Remarkably, however, when these systems are rapidly cooled, the CG's are supercooled even below the transition temperature and charge glass (CG) states result. In the CL and CG phases, anomalously slow charge fluctuations peculiar to glass are observed [4,5]; however, the CL and CG phases exhibit several orders of magnitude higher electrical conductivity than expected from the time scale of the charge fluctuations. In other words, the CL and CG states appear to possess dual characters of electrons, high itineracy as in typical organic conductors and glassy-like localization. How these contradictory characters cope with each other in a single material is a significant issue.

Previously, observing the Raman spectrum of the charge-sensitive mode ( $\nu_2$ ) in CL phase of  $\theta$ -RbZn where the central carbon site of the ET molecule was replaced with <sup>13</sup>C, we determined the charge density distribution through analyzing the spectral shape as described in the section on experimental methods. As a result, it was clarified that the CL phase of  $\theta$ -RbZn has a charge density profile having a peak at the  $\rho=0.5$  and continuously decreasing towards both sides of  $\rho=0$  and 1. It is expected that normal metals have a sharp peak at  $\rho=0.5$  and classical glass have sharp peaks at  $\rho=0$  and 1. The CL phase of  $\theta$ -RbZn is different from either, and there is no sign of phase separation between metal and classical glass. This result suggests that the charge location in the CG phase of  $\theta$ -RbZn is not particle-like but wave-like; so to speak, like a quantum glass.

The CG phase in  $\theta$ -TlCo, which has weaker charge frustration than  $\theta$ -RbZn, is of great interest to see the relation between the charge density profile and the degree of charge frustration. The CG phase of  $\theta$ -TlCo has, however, hardly been studied so far since  $\theta$ -TlCo has a lower glass-forming ability than  $\theta$ -RbZn and requires very high cooling speeds for quenching the high-temperature CL state. Here, we tried to realize the CG phase by applying the quenching technique developed in the Bi<sub>4</sub>I<sub>4</sub> experiment to  $\theta$ -TlCo and to investigate the charge density distribution in the CG phase of  $\theta$ -TlCo through analyzing the Raman spectrum.

## Experimental

Raman spectroscopy is a powerful method to investigate charge states in organic conductors. One of the Raman-active C=C stretching modes,  $\nu_2$ , is called the charge-sensitive mode, empirically known

that the peak wavenumber shifts linearly according to the valence of the molecule. That is

$$\nu = 1537\text{cm}^{-1} - 90\rho,$$

where  $\nu$  is the central wavenumber of the  $\nu_2$  mode, and  $\rho$  is the valence of the molecule. If  $\rho$  is distributed, the Raman spectrum is described as

$$I(\nu) = \int A(\rho)D(\rho)L(\nu - \nu'(\rho))d\rho,$$

where  $A$  is intensity when the valence of the molecule is  $\rho$ ,  $D$  is the charge distribution function, and  $L$  is the Lorenz function. The purpose of this study is to find the  $D$ . Transforming the above equation,  $D$  is described with the Fourier transform FT as

$$D = \frac{1}{A} \text{FT}^{-1} \left[ \frac{\text{FT}[I]}{\text{FT}[L]} \right].$$

To find  $D$ ,  $A$  is needed; however, since it is difficult to find the functional form of  $A$  theoretically, we determined  $A$  empirically. First, when the Raman spectrum of the CO phase of  $\theta$ -RbZn was examined, it was found that  $A$  cannot be represented linearly. Therefore, using three types of charge ordering materials with different charge distribution ratios,  $\theta$ -RbZn,  $\theta$ -TlCo, and  $\kappa$ -(ET)<sub>2</sub>Hg(SCN)<sub>2</sub>Cl, it was found that the Raman spectrum of the above substances can be reproduced best if  $A$  is decided as

$$A(\rho) = a\rho^n + b,$$

where  $a = 0.036$ ,  $b = 0.0022$ , and  $n = 3.77$ .

The single crystal of  $\theta$ -TlCo was prepared by the electrochemical oxidation method, and the C atoms in the center of the ET molecules were enriched with <sup>13</sup>C. The typical crystal size is ca. 0.5×0.5×0.1 mm<sup>3</sup>. The crystal was fixed with grease on a copper substrate, and the substrate was placed on a cooling stage Linkam 10002L with a glass window for optical observation. Raman spectra were collected with backscattering geometry using a Renishaw inVia Raman system. A 532 nm laser was used as the excitation light, and the light was focused by the objective lens Leica N Plan L50x. The scattered light through a grating with 1800 l/mm was detected by a charged-coupled device (CCD).

## Result and Discussion

Figure 3 shows typical Raman spectra of the equilibrium state of  $\theta$ -TlCo. A broad Raman spectrum is shown in the CL phase. This is due to the distribution of charge densities in the CL phase. In contrast, a spectrum with two sharp peaks is shown in the CO phase. This is because the sites are divided into two types, charge rich and poor, in the CO phase.

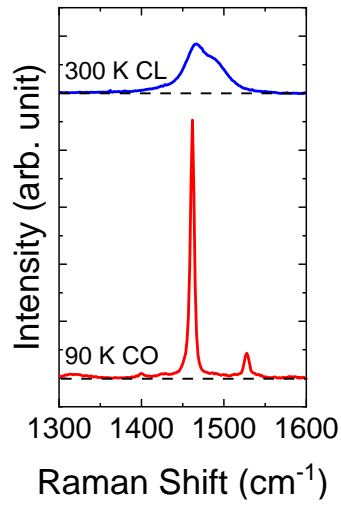


Figure 3 Raman spectra of  $\nu_2$  mode of the equilibrium states of  $\theta$ -TlCo. The blue line indicates the Raman spectrum at 300 K (CL) and the red line indicates the Raman spectrum at 90 K (CO).

An experimental setup as shown in Fig. 4 (a) is constructed to obtain the Raman spectrum of CG. After cooling to 90 K, a current of 0.43 A is applied to the heater ( $10.9 \Omega$ ) to heat a local region near the sample, and the current is cut off to quench this region. Figure 4 (b) shows the Raman spectra before, during, and after the current application. Raman spectrum of CO is observed before the current is applied, and CL is observed during the current application. Since the spectra before and after the current application coincide, CG is not formed even after quenching (Fig. 4 (c)). This is because the cooling rate is insufficient.

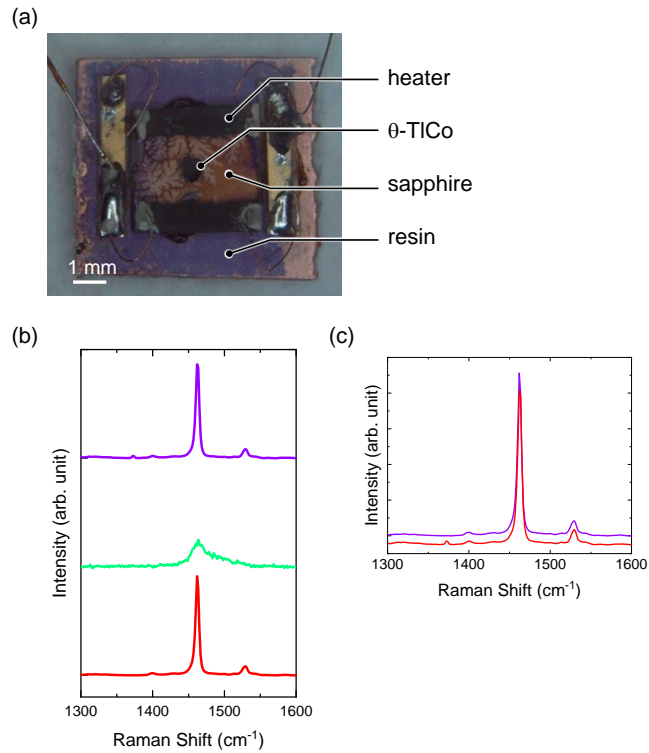


Figure 4 Rapid cooling of  $\theta$ -TiCo with a heater mounted on the substrate. (a) Sample photograph. A sapphire substrate is arranged on the resin substrate, and a heater and a sample are arranged on the sapphire substrate. The white line scale bar at the bottom left indicates 1 mm. (b) Raman spectra before (upper / purple), during (middle / green), and after (lower / red) current is applied to the heater. The Raman spectra of CO before and after the application of current and CL during application of current are shown. (c) Comparison of Raman spectra before and after applying current to the heater. Both Raman spectra coincide and show a Raman spectrum of CO.

For faster cooling, heating and cooling need to occur in a smaller area. Therefore, we tried to quench by directly applying a current pulse to the sample (Fig. 5 (a)). A load resistor (30 k $\Omega$ ) was placed in series with the sample to control the voltage applied to the sample (Fig. 5 (b)). A voltage of 40 V was applied for 1 second at 130 K. Figure 5 (c) shows an image after cooling to 90 K after applying a current and Raman spectra at several points. Figure 5(d) shows an image after heating to a temperature higher than the transition temperature and then slowly cooling to 90 K. These images were obtained by mapping in real space the integral values of the Raman spectrum in the range of 1460  $\text{cm}^{-1}$  to 1463  $\text{cm}^{-1}$ . The image immediately after the application of the current is clearly divided into two regions, a strong intensity region (red) and a weak intensity region (yellowish green). In the former, the Raman spectrum of CO is observed. In the latter, a Raman spectrum different from CO is observed, and there is no spatial dependence (Fig. 5 (e)). This spectrum is characterized by having a peak at almost the same wave number as the two peaks seen in the Raman spectrum of CO and a broad component

between the two wave numbers. Since this region is formed by rapid cooling and disappears when cooled again after the temperature rises above the transition temperature, it is considered that CG is formed in this region.

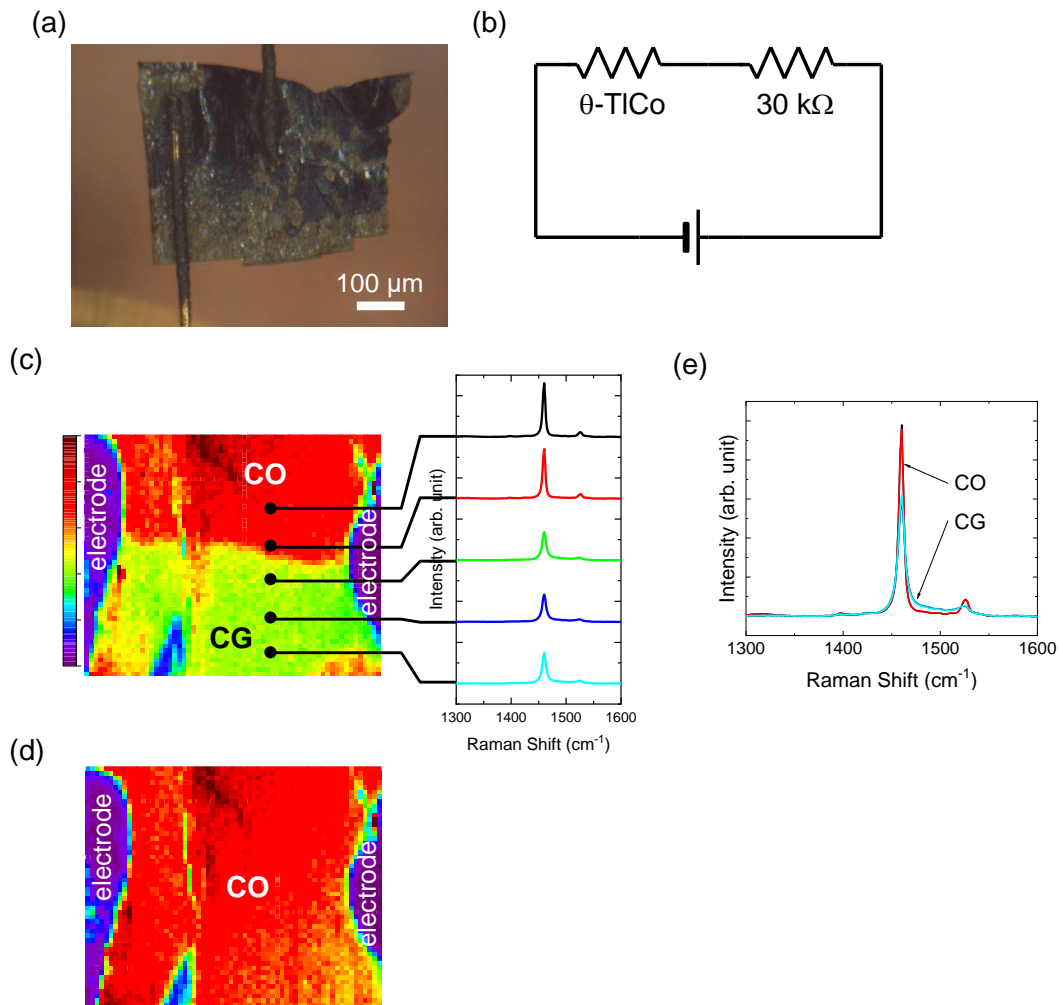


Figure 5 Rapid cooling of  $\theta$ -TlCo by applying an electric current directly to the sample. (a) Sample photograph. The white line at the bottom right is the scale bar which indicates 100  $\mu\text{m}$ . (b) Circuit diagram. A load resistor (30  $\text{k}\Omega$ ) is placed in series with the sample to suppress the voltage applied to the sample. (c) Image after application of pulse current and Raman spectrum of each point. (d) Image after the temperature is raised above the transition temperature and then slowly cooled to 90 K again after applying a current. See the text for how to map the c and d images. (e) Comparison of spectra in c. The two Raman spectra in the CO region and the three Raman spectra in the CG region are in good agreement with, respectively.

However, since the Raman spectrum of CG obtained here has characteristics of the Raman spectrum of CO, there is a possibility that CO is mixed in this region. If CO is mixed, it is expected that CO will

be mixed in different ratios if it is rapidly cooled by different methods, so the Raman spectrum of CG obtained here should not be reproduced. Therefore, we attempted rapid cooling by irradiating the sample surface with a laser for a short time to instantly heat and cool it and investigated whether CO is mixed in this Raman spectrum.

The focus was moved 50  $\mu\text{m}$  away from the sample surface and a 2.3 W laser was irradiated for 0.5 seconds at 90 K. Figure 6 (b) and (c) show images immediately after irradiation and after the sample was heated to a temperature higher than the transition temperature and then slowly cooled to 90 K again. These images were obtained in the same way as in Fig. 5. In Fig. 6 (b), there is a circular region (yellow) with low intensity in the region with high intensity (red). The former is the area irradiated with the laser. Since the former disappears when the temperature was raised and then cooled again (Fig. 6 (c)), it is considered that CG was formed in the former. In addition, since the Raman spectrum in this region and the current pulse obtained coincide with each other as shown in Fig. 6 (d), these are pure CG Raman spectra without CO.

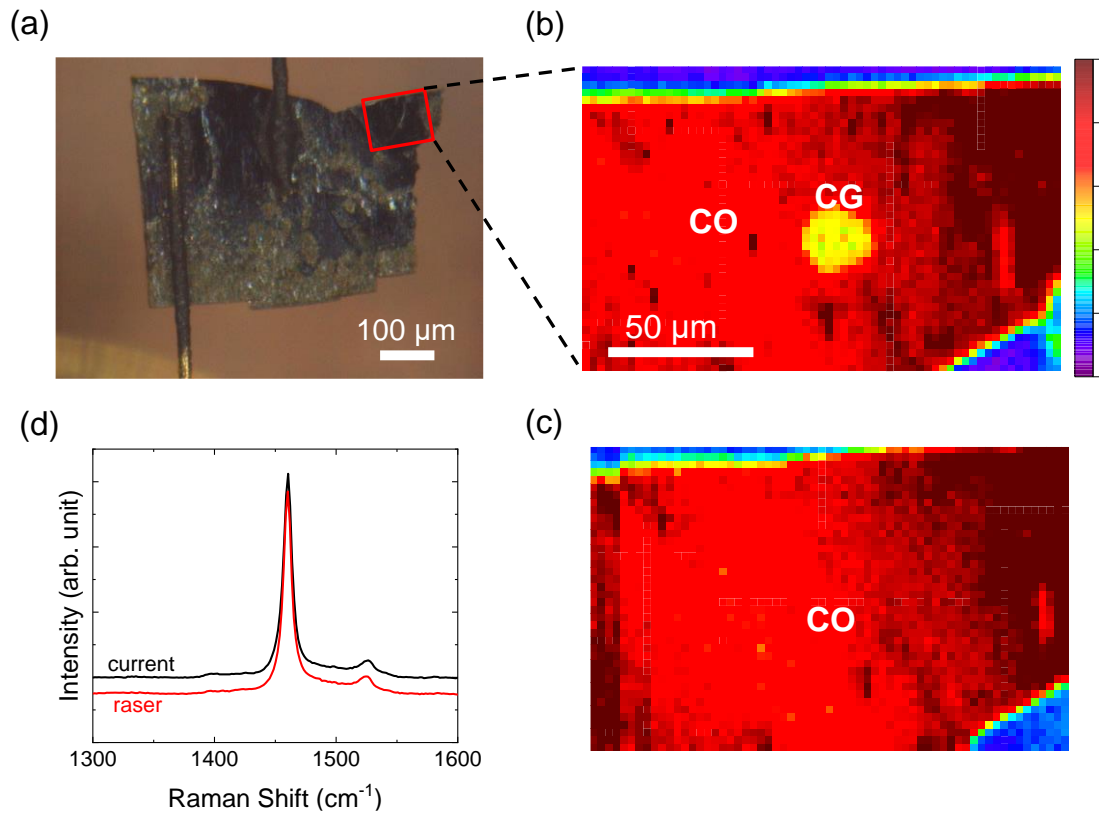


Figure 6 Laser quenching of  $\theta$ -TiCo. (a) Sample photograph. The white line at the bottom right is the scale bar which indicates 100  $\mu\text{m}$ . The red square line indicates the area where the image is acquired with b and c. (b) Image after laser irradiation. The white line at the bottom left is the scale bar which indicates 50  $\mu\text{m}$ . (c) Image after the sample was heated to a temperature higher than the transition temperature and then slowly cooled to 90 K again. See the main text for how to map the b and c images. (d) Comparison of Raman spectra of CG obtained by current pulse and laser. The two spectra are in good agreement.

The charge density distribution is calculated from the Raman spectra of CO and CG (Fig. 7). In CO, the site is divided into charge rich and poor, and two corresponding peaks appear. In CG, in addition to the broad component around  $\rho=0.5$ , a peak corresponding to charge rich and poor such as CO appears. Therefore, the CG phase of  $\theta$ -TiCo is close to the state where the site is divided into charge rich and poor, and the charge is particle-like. Since CG does not have the long-range order, the CG phase of  $\theta$ -TiCo can be regarded as a particle-like and disordered state of charge. This is close to classical glass.

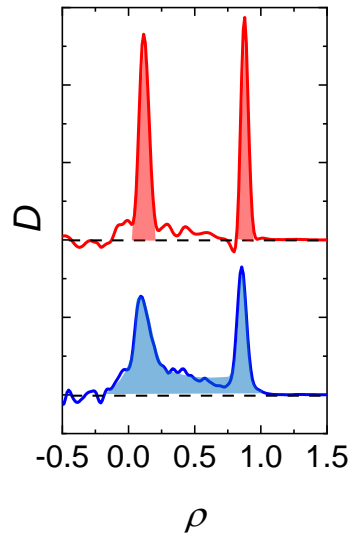


Figure 7 CO and CG charge density distribution. The charge density distribution of CO is indicated by the red line, and that of CG is indicated by the blue line.

## Conclusion

$\theta$ -TlCo has the weak charge frustration and low glass-forming ability among the known  $\theta$ -(ET)<sub>2</sub>X. In this study, we succeeded in forming the CG phase of  $\theta$ -TlCo by two methods, current pulse and laser, measured the Raman spectrum of  $\nu_2$  mode, analyzed it to obtain the charge density distribution. As a result, it revealed that the CG phase of  $\theta$ -TlCo is closer to classical glass than that of  $\theta$ -RbZn. This result suggests that the nature of the CG phase changes from classical to quantum as the frustration increases.

## Acknowledgements

We would like to thank my advisors, Professor Kanoda, Associate Professor Kagawa, Assistant Professor Oike, and Professor Hasegawa, for their support and cooperation in this research. We would like to thank my sample provider, Associate Professor Sasakawa of Tokyo Institute of Technology. We would like to thank MERIT for the opportunity to conduct this research.

## Literature

- [1] G. Autes, *et al.*, *Nat. Mater.* **15**, 154 (2016).
- [2] R. Noguchi, *et al.*, *Nature* **566**, 158 (2019).
- [3] X. Wang, *et al.*, *Phys. Rev. B* **98**, 174112 (2018).
- [4] F. Kagawa, *et al.*, *Nat. Phys.* **9**, 2642 (2013).
- [5] T. Sato, *et al.*, *Phys. Rev. B* **89**, 121102(R) (2014).